PERGAMON

Computers and Structures 74 (2000) 215–231

Computers & Structures

www.elsevier.com/locate/compstruc

Using finite element analysis for simulation of reliability tests on solder joints in microelectronic packaging

Cemal Basaran[a,*], Rumpa Chandaroy[b,1]

[a]*Department of Civil, Structural and Environmental Engineering, SUNY at Buffalo, 212 Ketter Hall, Buffalo, NY 14260-4300, USA*
[b]*HKS ABAQUS Inc., Detroit, MI, USA*

Received 12 August 1997; accepted 27 October 1998

Abstract

In the microelectronics industry tin/lead solder joints are an essential part of packaging. It is well established that heat generated by the circuits when the device is on leads to a thermal loading which is cycling in nature. Due to the coefficient of thermal expansion (CTE) mismatch between the bonded layers, the solder joint experiences cycling shear strain, which leads to short cycle fatigue. When semiconductor devices are used in a vibrating environment, additional strains shorten the fatigue life of a solder joint. Reliability of these joints in new packages is determined by laboratory tests. In order to use the FEM to replace these expensive reliability tests, a unified constitutive model for Pb40/Sn60 solder joints has been developed and implemented in a thermo-viscoplastic-dynamic finite element procedure. The model incorporates thermal-elastic-viscoplastic and damage capabilities in a unified manner. The constitutive model has been verified extensively against laboratory test data. The finite element procedure was used for thermo-viscoplastic, dynamic and coupled thermo-viscoplastic-dynamic analyses for fatigue life predictions. The results indicate that using Miner's rule to calculate accumulative damage by means of two separate analyses, namely dynamic and thermo-mechanical, significantly underestimates the accumulative total damage. It is also shown that a simultaneous application of thermal and dynamic loads significantly shortens the fatigue life of the solder joint. In the microelectronic packaging industry it is common practice to ignore the contribution of vibrations to short cycle fatigue life predictions. The results of this study indicate that damage induced in the solder joints by vibrations has to be included in fatigue life predictions to accurately estimate their reliability.

Keywords: Disturbed state concept; Viscoplasticity; Vibration; Thermal cycling; Solder joints; Microelectronic packaging

1. Introduction

Among all the bonding technology options in the electronics industry surface mount technology (SMT) is the fastest growing. This popularity is due to the fact that by providing more space, SMT increases the I/O interconnection density. The down side of using SMT is that the solder joints are susceptible to thermal fatigue. As a result, the reliability of surface mount components has become a critical issue. The main reason for the low cycle thermal fatigue of solder joints is the CTE mismatch between the joined components. Semiconductor devices experience temperature variations which are caused either by heat dissipation from

* Corresponding author. Tel.: +1-716-645-2114/2429; fax: +1-716-645-3733.
E-mail address: cjb@eng.buffalo.edu (C. Basaran)
[1] Formerly Ph.D. student at SUNY at Buffalo

0045-7949/00/$ - see front matter
PII: S0045-7949(99)00028-0

the circuits, or by ambient temperature changes. Because of the CTE mismatch, different elongations and contractions take place in the layers. As a result, the solder joint between the layers experiences cycling shear strain and creep damage [49].

When semiconductor devices are used in a vibrating environment, dynamic strains contribute to the failure mechanism and can sometimes become the cause for dominant failure. Presently in the microelectronics industry, all vibration induced stresses on solder joints are considered to be elastic. It is assumed that there is no contribution to the low cycle fatigue life from vibrations [4]. In this paper it is shown that vibration effects cannot be classified categorically as elastic only and ignored in low cycle fatigue studies. It is also shown that at elevated temperatures, irreversible strains due to vibrations are greatly amplified. In this study it was observed that even the dynamic loads that are too small to induce irreversible deformations, can induce significant damage when coupled with thermal cycling.

A unified damage mechanics-based constitutive model has been developed and then implemented in a nonlinear finite element analysis procedure for fatigue life analysis under coupled dynamic and thermal loads. The purpose of the study has been to observe the contribution of thermal and vibration induced strains to the fatigue life of solder joints. The fatigue life of the solder joint was determined by Miner's rule and also by coupled finite element analyses. For Miner's rule the damage due to each load type acting individually was determined and then superposed to assess the overall fatigue life of the joint. It should be pointed out that Miner's rule is commonly used in the industry [4,38,50]. In coupled analyses both vibrations and thermal cycling were applied simultaneously and the fatigue life was directly computed by the finite element code.

A number of researchers have proposed constitutive models for Pb/Sn solder alloys. Some of them are Refs. [4,6,7,15,20,21,24,26,27,29,31,34,35,39,41–48,51–53] and others. A common shortfall of these models is that most are empirical in nature and do not include the grain size and microstructural changes that occur in a Pb40/Sn60 solder during thermo-mechanical fatigue, Frear et al. [25,26].

Most of these models require using empirical curves, e.g. Coffin [17,18] and Manson [36,37], in determining the number of cycles to failure rather than determining the fatigue life at the constitutive level. In the proposed model, the entropy of the solder joint is used to quantify the damage in the material. Hence, the fatigue life is determined at the stress analysis level rather than in a separate fatigue analysis. This integrated analysis approach significantly reduces the analysis time.

2. Material model

The constitutive model proposed in this paper is based on the disturbed state concept (DSC). The DSC has been used extensively for modeling geomaterials, concrete, metals and alloys [5–9,11,22,23]. The DSC is a material modeling approach which treats the continuum as an inhomogeneous mixture rather than as a homogeneous medium. According to the DSC, the continuum is composed of intact and fully adjusted parts. The intact part represents the virgin material reference state. The fully adjusted part represents the material that is in the residual asymptotic reference state. The fully adjusted part can be assigned different reference states for different materials. In this study it is assumed that in the fully adjusted state, the material cannot carry any shear stress but can carry hydrostatic compressive stresses only. We will refer to this particular definition of the fully adjusted state as the damaged state.

Initially the material is mostly in the intact state. During service the volume of the material in the intact state decreases and the volume of the material in the damaged state increases. As a result, the response of the material is defined by a volume weighted average of the response of the intact part and the response of the damaged part. The response of the material in the intact part will be different than in the damaged part. In general, stresses will be higher in the intact part and strains will be higher in the damaged part. In the DSC continuum due to a stress differential between the damaged and the intact parts, a material moment is introduced at the constitutive equation level, similar to Cosserat's continuum [19]. Furthermore, due to having different strains in the damaged and the intact parts, there is a relative strain which accounts for an additional energy dissipation mechanism. As a result the DSC enables us to account for three separate energy dissipation mechanisms in the material. The incremental stress-strain relation in the DSC can be given by [6,22,30]:

$$\mathrm{d}\sigma_{ij}^{\mathrm{a}} = C_{ijkl}^{\mathrm{DSC}}\,\mathrm{d}\varepsilon_{kl}^{\mathrm{i}} \tag{1}$$

where $\mathrm{d}\sigma_{ij}^{\mathrm{a}}$ is the incremental average stress tensor, $\mathrm{d}\varepsilon_{kl}^{\mathrm{i}}$ is the incremental strain tensor for the intact part, and the DSC tangential constitutive tensor is given by:

$$C_{ijkl}^{\mathrm{DSC}} = \lfloor (1-D)^{i}C_{ijkl}^{\mathrm{evp}\theta} + D(1+\alpha)^{\mathrm{c}}C_{ijkl}^{\mathrm{evp}\theta} + (\sigma_{ij}^{\mathrm{c}} - \sigma_{ij}^{\mathrm{i}})R_{kl} \rfloor \tag{2}$$

where ${}^{\mathrm{i}}C_{ijkl}$ and ${}^{\mathrm{c}}C_{ijkl}$ are the tangential constitutive tensors for the intact and damaged parts, respectively, σ_{ij}^{c} and σ_{ij}^{i} are the total stress tensors for the damaged and intact parts, respectively, D is the accumulative

damage, α is the empirical relative strain coefficient, and R_{kl} is the material moment tensor.

In this proposed model a damage criterion based on the second law of thermodynamics and statistical continuum mechanics is used. The damage model utilizes entropy, which is a measure of disorder in the system as a damage metric [10,13], using statistical mechanics, gave a precise meaning to disorder and established the connection between disorder and entropy by the following equation:

$$s = k \ln w \tag{3}$$

where s is the entropy, k is Boltzmann's constant and w is the disorder parameter which is the probability that the system will exist in the state it is in relative to all the possible states it could be in. 'This equation connects a thermodynamic and macroscopic quantity, the entropy, with a statistical microscopic quantity, the probability' [28].

The entropy in the context of the Helmholtz free energy function is given by:

$$\phi = e - \theta s \tag{4}$$

where ϕ is the Helmholtz free energy, e is the internal energy, θ is the absolute temperature and s is the entropy.

If we select an initial reference state of the material as state 'o', then change in the disorder at any arbitrary time with respect to the initial reference state can be given by

$$\Delta W = W_{\mathrm{o}} - W = \mathrm{e}^{(e_{\mathrm{o}}-\phi_{\mathrm{o}})/(N_{\mathrm{o}}k\theta_{\mathrm{o}}/\bar{m}_{\mathrm{s}})} - \mathrm{e}^{(e-\phi)/(N_{\mathrm{o}}k\theta/\bar{m}_{\mathrm{s}})} \tag{5}$$

Using the definitions given in Eqs. (3) and (4) and also using the fundamental thermodynamic relations yields the following damage evolution function:

$$D = 1 - \mathrm{e}^{-(\Delta e-\Delta\phi)/(N_{\mathrm{o}}k\theta/\bar{m}_{\mathrm{s}})} \tag{6a}$$

where

$$\Delta e - \Delta\phi = \frac{1}{\rho}\left(\int_{\varepsilon_{\mathrm{o}}}^{\varepsilon} \sigma_{ij}\,\mathrm{d}\varepsilon_{ij}^{\mathrm{in}}\right) - \frac{1}{\rho}\int_{t_{\mathrm{o}}}^{t} \frac{\partial q_i}{\partial x_i}\,\mathrm{d}t + \int_{t_{\mathrm{o}}}^{t} \dot{\gamma}\,\mathrm{d}t \tag{6b}$$

where σ_{ij} is the total stress tensor, $\mathrm{d}\varepsilon_{ij}^{\mathrm{in}}$ is the incremental inelastic strain tensor, ρ is the unit mass density, q_i is the heat flux vector, $\dot{\gamma}$ is the distributed internal heat production rate per unit mass and $\mathrm{d}t$ is the time increment.

The yield surface, F, in the proposed constitutive model is given by [14]:

$$F = \frac{J_{2\mathrm{D}}}{P_{\mathrm{a}}^2} - k\frac{(J_1 + R(\theta))^2}{P_{\mathrm{a}}} \tag{7}$$

where J_1 is the first invariant of the total stress tensor, $J_{2\mathrm{D}}$ is the second invariant of the deviatoric stress tensor, P_{a} is the atmospheric pressure, $R(\theta)$ is the material bonding stress, and k is the isotropic hardening parameter.

3. Thermo-elasto-viscoplasticity

In service, Pb/Sn solder joints operate at high homologous temperature (0.65 T_{m}), which is defined by T_{use} (K)/T_{melt} (K). Therefore, the contribution of creep to the fatigue damage becomes very significant. As a result, using a viscoplastic model for the characterization of the thermo-mechanical behavior of the Pb/Sn solder alloy is essential. Assuming small strains, the total strain increment tensor for a thermo elasto-viscoplastic problem can be separated into three parts:

$$\mathrm{d}\varepsilon_{ij} = \mathrm{d}\varepsilon_{ij}^{\theta} + \mathrm{d}\varepsilon_{ij}^{\mathrm{e}} + \mathrm{d}\varepsilon_{ij}^{\mathrm{vp}} \tag{8}$$

where $\mathrm{d}\varepsilon_{ij}^{\theta}$, $\mathrm{d}\varepsilon_{ij}^{\mathrm{e}}$, and $\mathrm{d}\varepsilon_{ij}^{\mathrm{vp}}$ are the incremental thermal, elastic and viscoplastic strain tensors, respectively. The thermal strain increment is defined by:

$$\mathrm{d}\varepsilon_{ij}^{\theta} = \alpha_{\mathrm{T}}\,\mathrm{d}\theta I_{ij} \tag{9}$$

where α_{T} is the coefficient of thermal expansion, $\mathrm{d}\theta$ is the increment of temperature, and I_{ij} is the unit vector. The elastic strain increment is defined by:

$$\mathrm{d}\varepsilon_{ij}^{\mathrm{e}} = D_{ij}^{\mathrm{e}}\,\mathrm{d}\sigma_{ij} \tag{10}$$

where D_{ij}^{e} is the inverse of the elastic constitutive tensor. In order to define the increment of the viscoplastic strain in Eq. (8) we need to define a viscoplastic strain rate function. Tin/lead solder is a two phase alloy with an evolving microstructure. Chandaroy [14] has shown that the microstructure and grain size of a solder joint depends on its cooling rate, age, temperature and strain history. There are plenty of creep rate functions proposed in the literature for Pb/Sn solder alloys. For an extensive review see Ju et al. [32]. For Pb/Sn solder alloys, the creep function used must take into account the microstructure. Yet it should be simple enough to be used in a boundary value problem. For the constitutive model proposed in this paper the following strain rate function was adopted by Chandaroy [14]:

$$\dot{\varepsilon}_{ij}^{\mathrm{vp}} = A(\sinh[B\bar{\sigma}])^n (d)^m \exp\left[\frac{-Q}{k\theta}\right]\frac{\partial\bar{\sigma}}{\partial\sigma_{ij}} \tag{11}$$

where A, B, n and m are material constants, σ is the von Mises equivalent stress and is given by $\bar{\sigma} = \sqrt{(3J_{2\mathrm{D}})}$, d is the average solder grain size, Q is the creep activation energy, k is the Boltzmann's constant, θ is the absolute temperature in Kelvin, and σ_{ij} is the total stress tensor.

Implementing the definitions given by Eqs. (9)–(11) and using Taylor's series expansion and time integration on Eq. (11) finally yields the incremental stress–strain relation for the thermo-elasto-viscoplastic case below:

$$(\mathrm{d}\sigma_{ij})_n = (C^{\mathrm{evp}\theta}_{ijkl})_n (\mathrm{d}\bar{\varepsilon}_{kl})_n \tag{12}$$

$$(C^{\mathrm{evp}\theta}_{ijkl})_n = [[C^{\mathrm{e}\theta}_{ijkl}]^{-1} + \Delta t\chi[G_1]_{ijkl}]^{-1}_n \tag{13a}$$

and

$$(\mathrm{d}\bar{\varepsilon}_{ij})_n = \lfloor \mathrm{d}\varepsilon_{ij} - \Delta t\dot{\varepsilon}^{\mathrm{vp}\theta}_{ij} - \Delta t\chi[G_2]_{ij}\,\mathrm{d}\theta - \alpha_{\mathrm{T}}\,\mathrm{d}\theta I_{ij}\rfloor_n \tag{13b}$$

where Δt is the time increment for the viscoplastic strain rate integration, χ is the time integration coefficient, $[G_1]$ is the first derivative of the viscoplastic strain rate function with respect to total stress, and $[G_2]$ is the first derivative of the viscoplastic strain rate function with respect to temperature.

4. Verification of the material model

The constitutive model proposed in this study was verified against test data reported in the literature. Adams [3] performed a series of tensile tests on Pb40/Sn60 bulk solder specimen using an Instron 1122 testing machine. These tests were performed at a constant crosshead speed, but since only a small strain was applied, this was assumed to be an approximately constant true strain rate. The tests were performed at constant temperatures between −55 and 125°C over a range of strain rates from 8.33×10^{-5} to 8.33×10^{-2}. The specimens were 60/40 tin/lead solder. The solder specimen average grain size was not reported by the author. Since Adams' [3] creep rate versus stress curve data lies between the two creep curves (of grain size 9.7 and 28.4 μm) of Kashyap and Murty's [33] data, a 15 μm grain size was assumed. The values of Young's modulus of $E(\mathrm{GPa}) = 62.0–0.067\theta$ was obtained from ultrasonic testing on bulk Pb40/Sn60 solder samples. Fig. 1 compares the constitutive model results with test data at 22°C for different strain rates. Figs. 2–4 present a comparison of stress versus strain results at different temperatures and strain rates at 1.67×10^{-2}, 1.67×10^{-3}, and 1.67×10^{-4}, respectively. Comparisons with test data indicate that the constitutive model can predict the material behavior reasonably well, especially for small strain rates. The main difference between the test data and the simulation occurs during the hardening zone of the curves. The development of a better hardening model is presently underway.

5. Finite element procedure implementation

Most commercially available FEM codes such as ABAQUS [2], ANSYS [1], etc. cannot perform a damage mechanics analysis for a dynamic problem using a viscoplastic material model. Hence, implementing the models in an FEM code was essential. For the displacement based FEM, the equilibrium equation in incremental form is given by [12]:

$$\Sigma\int_V [B]^{\mathrm{T}}\{\mathrm{d}^r\sigma^{\mathrm{a}}_n\} = \{Q_{n+1}\} - \Sigma\int_V [B]^{\mathrm{T}}\{^r\sigma^{\mathrm{a}}_n\} \tag{14}$$

where $[B]$ is the strain–displacement transformation matrix, $\{\mathrm{d}\sigma^{\mathrm{a}}\}$ is the average stress vector increment, V is the volume, n is the load step number, r is the iteration number and $\{Q_{n+1}\}$ is the vector of nodal external loads. Implementing the DSC formulation in Eq. (14), introducing inertia, damping forces and using Newmark's implicit scheme (with coefficients $\delta = \frac{1}{2}$ and $\alpha = \frac{1}{4}$) for a time domain integration of the equation of motion yields the following finite element equilibrium equation:

$$\begin{aligned}
&[^{r-1}\hat{K}_n]\{^r\,\mathrm{d}q_{n+1}\} = \{Q_{n+1}\} - \int_V [B]^{\mathrm{T}}[^{r-1}\sigma^{\mathrm{a}}_n]\\
&\mathrm{d}V - \int_V [B]^{\mathrm{T}}\{^{r-1}\sigma^{\mathrm{c}}_n - ^{r-1}\sigma^{\mathrm{i}}_n\} \quad \mathrm{d}D_n\\
&\mathrm{d}V + \int_V \Delta t_n[B]^{\mathrm{T}}[^{r-1}L^{\exp\theta}_n]\{^{r-1}\varepsilon^{\mathrm{vp}\theta}_n\}\,\mathrm{d}V + \int_V \Delta t_n\chi\\
&\mathrm{d}\theta[B]^{\mathrm{T}}[^{r-1}L^{\mathrm{evp}\theta}_n][^{r-1}G_2]_n\{\bar{\imath}\}\,\mathrm{d}V + \int_V \alpha_{\mathrm{T}}\\
&\mathrm{d}\theta[B]^{\mathrm{T}}[^{r}L^{\mathrm{evp}\theta}_n]\{\bar{\imath}\}\\
&\mathrm{d}V - [M]\left\{\frac{4}{\Delta t^2_{\mathrm{d}}}(^{r-1}q_{n+1} - q_n) - \frac{4}{\Delta t_{\mathrm{d}}}\dot{q}_n - \ddot{q}_n\right\}\\
&- [C_n]\left\{\frac{2}{\Delta t_{\mathrm{d}}}(^{r-1}q_{n+1} - q_n) - \dot{q}_n\right\} - [M]\{\ddot{q}_g\}_{n+1}
\end{aligned} \tag{15}$$

where

$$[^{r-1}\hat{K}_n] = [M]\frac{4}{\Delta t^2_{\mathrm{d}}} + [C_n]\frac{2}{\Delta t_{\mathrm{d}}} + [^{r-1}K_n] \tag{16}$$

$$[^{r-1}K_n] = \int_V [B]^{\mathrm{T}}[^{r-1}L^{\mathrm{evp}\theta}_n][B]\,\mathrm{d}V \tag{17}$$

$$\begin{aligned}
[^{r-1}L^{\mathrm{evp}\theta}_n &= [(1 - D_n)[^{\mathrm{i}}_{r-1}C^{\mathrm{evp}\theta}_n] + D_n(1+\alpha)\\
&\times [^{\mathrm{c}}_{r-1}C^{\mathrm{evp}\theta}_n]
\end{aligned} \tag{18}$$

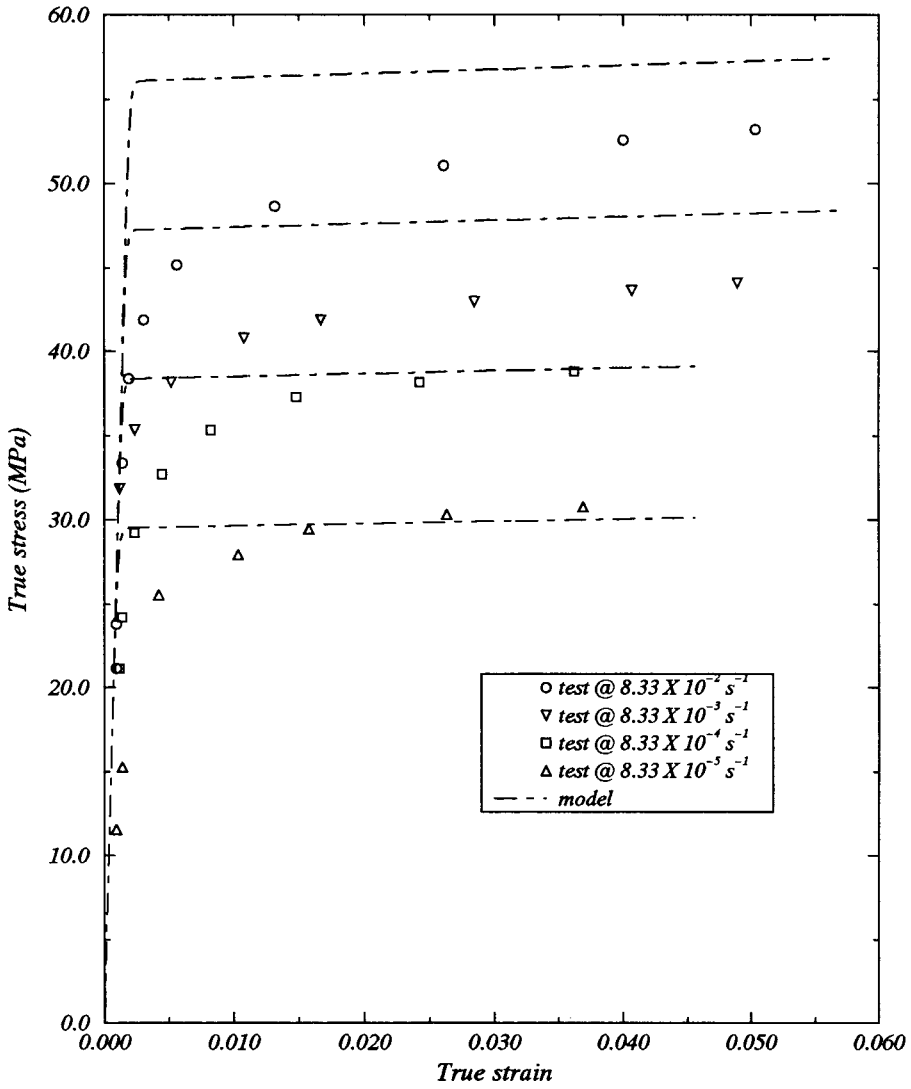

Fig. 1. Comparison of axial stress versus axial strain response at different strain rates at 22°C.

$$[C] = \alpha_1[M] + \alpha_2[K] \tag{19}$$

and where $\{d^r q_{n+1}\}$ is the vector of nodal displacement increments, Δt_n is the time step for viscoplasticity time integration, $\{q\}$, $\{\dot{q}\}$, $\{\ddot{q}\}$ are the nodal displacement, nodal velocity and nodal acceleration vectors, respectively $\{\ddot{q}_g\}$ is the base acceleration vector, $[M]$ is the mass matrix , $[C]$ is the damping matrix, α_1 and α_2 are the Rayleigh damping coefficients, and $[K]$ is the stiffness matrix.

The convergence to a steady-state solution in viscoplastic problems can be monitored by checking the viscoplastic strain rate during each time step [40]:

$$\begin{bmatrix} \Sigma & \{\Delta\varepsilon_n^{vp\theta}\} \\ \Sigma & \{\Delta\varepsilon_1^{vp\theta}\} \end{bmatrix} \times 100 < \text{tolerance} \tag{20}$$

For dynamic equilibrium, convergence is checked with the following criteria [12]

$$\frac{\|\{^{r-1}F_{n+1}\} - [M]\{^{r-1}\ddot{q}_{n+1}\} - [C]\{^{r-1}q_{n+1}\}\|_2}{RNORM} \leq RTOL \tag{21}$$

and

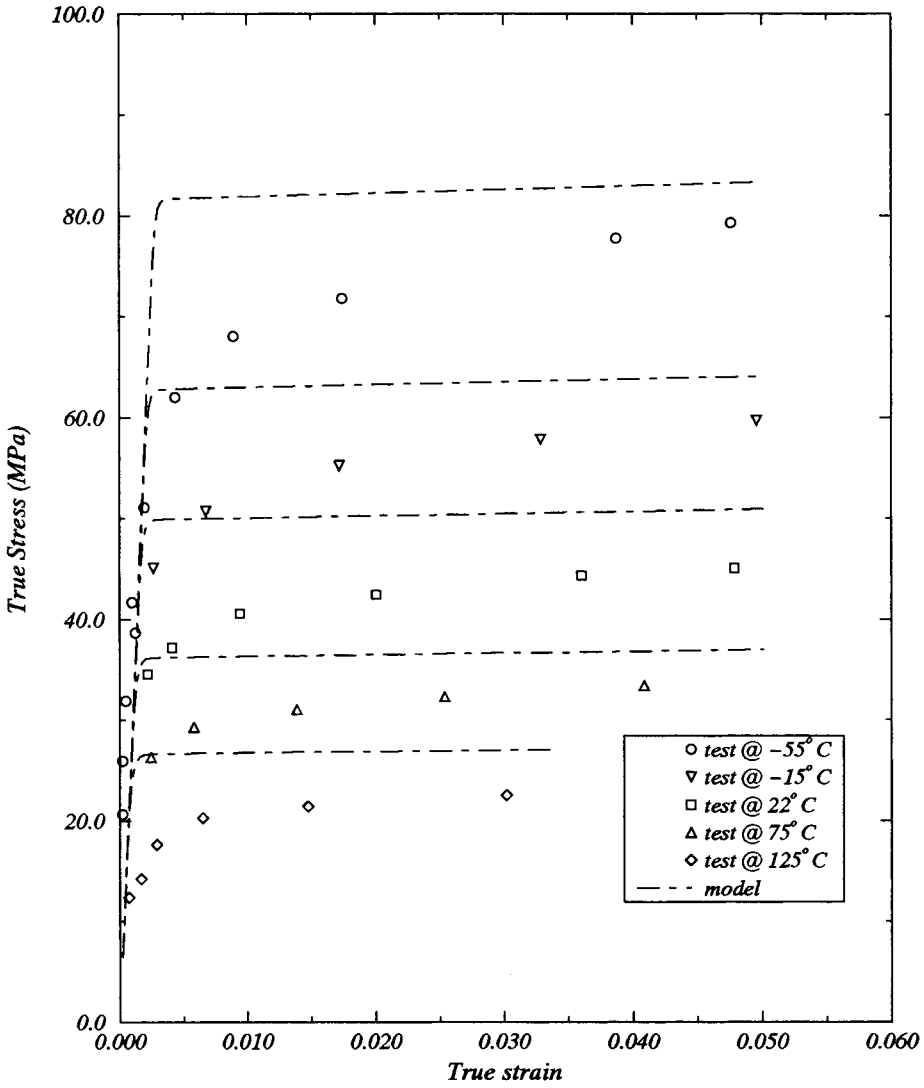

Fig. 2. Comparison of stress versus strain response at different temperatures, strain rate = 1.67×10^{-2}/s.

$$\frac{\mathrm{d}^r q_n \lfloor \{^{r-1}F_{n+1}\} - [M]\{^{r-1}\ddot{q}_{n+1}\} - [C]\{^{r-1}q_{n+1}\} \rfloor}{\mathrm{d}^1 q_n [\{F_n\} - [M]\{\ddot{q}_n\} - [C]\{\dot{q}_n\}]} \leq ETOL \tag{22}$$

6. Analysis of a solder joint between a ceramic chip carrier and a printed wiring board

The fatigue life and stress–strain response of a Pb40/Sn60 solder joint in a surface mount technology package subjected to thermal cycling and vibrations is studied. The package shown in Fig. 5 was subjected to a temperature cycling and base acceleration. The time histories of the temperature cycling and the vibrations are given in Figs. 6 and 7, respectively.

Both low and high cycle fatigue were considered, since under dynamic loading, the behavior of the solder alloy can be elastic or inelastic depending on the acceleration and the frequency of the vibrations. For low cycle fatigue (up to 10^4 cycles [4]), the damage was calculated using Eq. (6). For high cycle fatigue (over 10^4 cycles [4]), the damage was calculated using the following criterion [4]:

$$D = \Sigma(n_i/N_i) \tag{23}$$

where n_i is the number of cycles experienced and N_i is

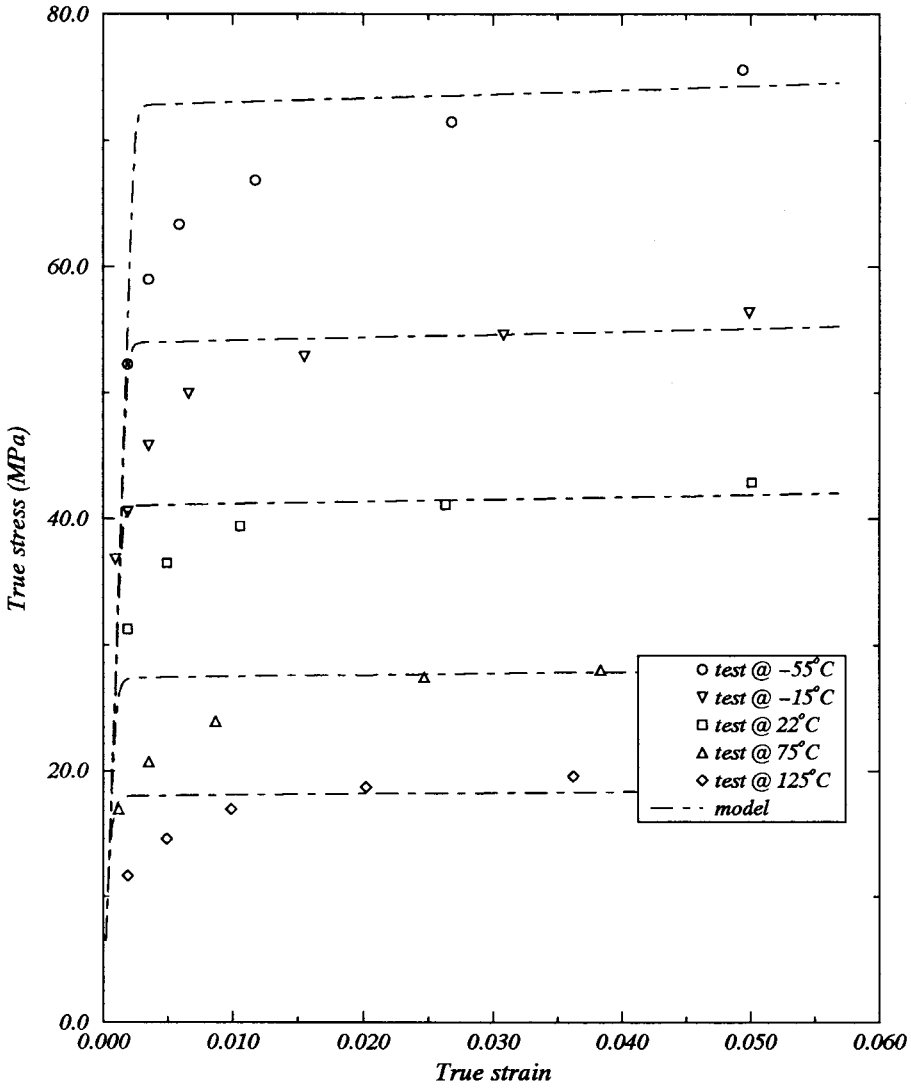

Fig. 3. Comparison of stress versus strain response at different temperatures, strain rate = 1.67×10^{-3}/s.

the total number of cycles to failure. High cycle fatigue life test data was obtained from the data presented by Steinberg [50].

The combined loading situation is first simulated by superposing the damage due to vibration and thermal loads using Miner's rule. The damage due to each loading type acting alone is determined and then superposed to assess the overall fatigue life of the joint [40]. In the second stage, coupled thermo-viscoplastic-dynamic analyses are performed using the finite element procedure presented above, in which the total damage is computed directly.

In the literature and in the industry it is common practice to compute the total fatigue damage caused by vibration and thermal cycling using Miner's rule [4]. A finite element analysis was conducted for three separate load combinations. Fatigue life study results for these load cases are presented below.

6.1. Load case I

This load case consists of thermal cycling between −25 and 100°C and 5 $g-10$ Hz vibrations in the X-direction (horizontal axis in the figure plane) only. Fig. 8 shows the shear stress–shear strain response of the solder joint for 5 g–10 Hz vibrations only at room temperature (25°C). The response is elastic after 120 cycles of dynamic loading. A thermal analysis alone was also performed on the package for the time history shown in Fig. 6. The stresses in the solder joint were

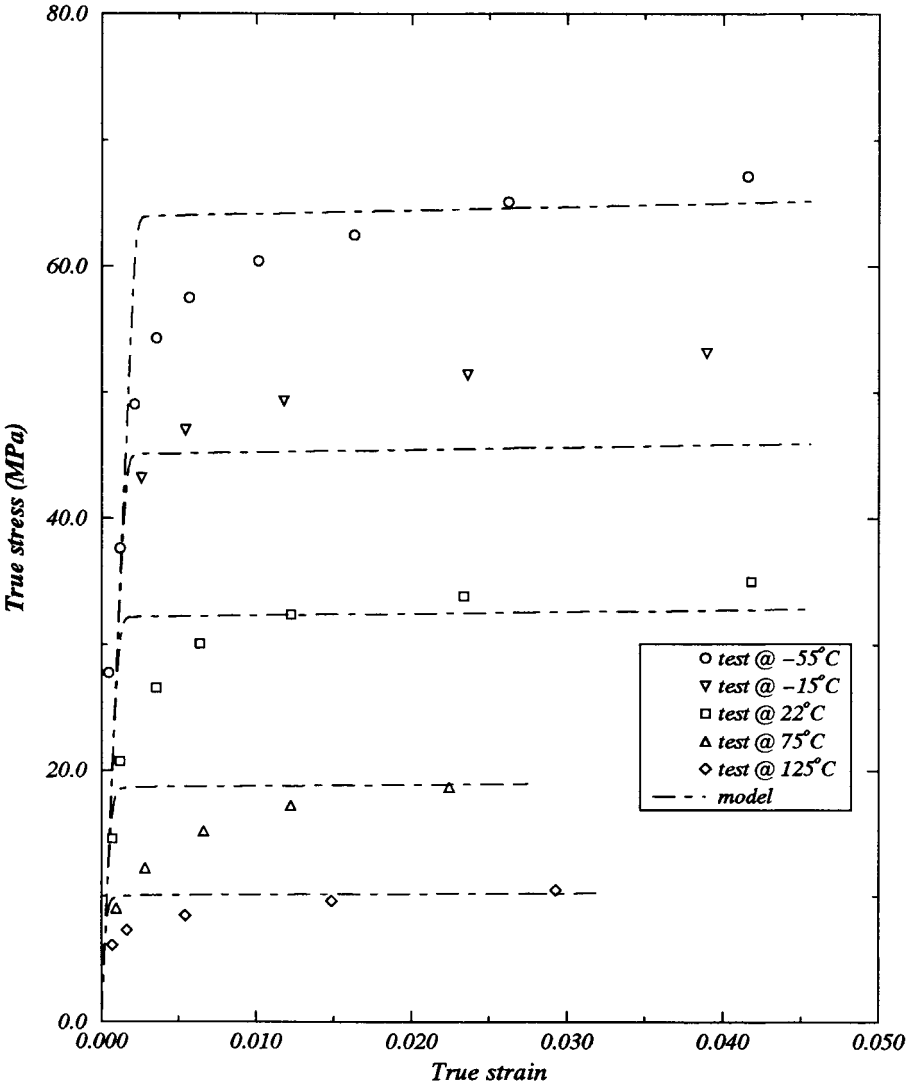

Fig. 4. Comparison of stress versus strain response at different temperatures, strain rate = 1.67×10^{-4}/s.

observed to be very small. The reason for this could be the very short period of the thermal cycle. Since the main factor that induces damage in the Pb/Sn solder joint is the creep damage, the 12 s loading is not long enough to induce any significant creep damage [5]. Basaran et al. [6] have shown that thermal cycles with long periods induce significant creep-damage. Fig. 9 shows the response of the Pb40/Sn60 solder joint under simultaneous thermal and dynamic loading. As

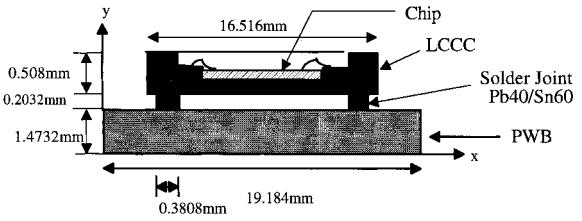

Fig. 5. A schematic of the surface mount technology package.

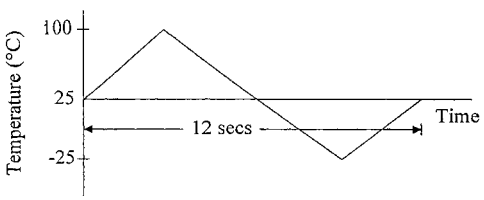

Fig. 6. Time history of thermal loading.

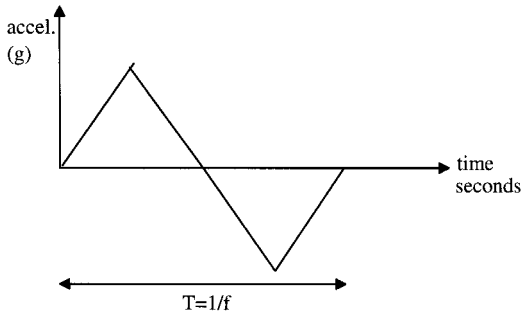

Fig. 7. Time history of dynamic loading.

can be seen from the figure, there is significant plasticity under concurrent loading, even though stresses and strains on the older joint are negligible when only thermal loading is applied to the package for 12 s. The main cause for this behavior is the degradation of material properties (in particular Young's modulus) under higher temperatures. As the temperature increases, the plastic strain level starts to increase and the area inside the stress–strain curve becomes bigger. The outer most curve represents the 30th dynamic cycle, at which point the temperature is maximum. As the temperature begins to decrease below 100°C, the plastic strain level begins to reduce, and then goes back to the original position at room temperature. The cooling zone of the temperature cycle also induces plastic deformation in the solder joint, albeit significantly less than above room temperatures, due to the fact that Young's modulus increases below room temperatures. It is important to point out that, due to the cyclic nature of the loading, the plastic strain induced in the higher temperatures is reversed for the cooling period. As a result, the final plastic strain is very small, although the actual damage induced in the system is significant. The stress level during concurrent loading does not change much. This is because it usually takes many more thermal cycles or longer hold times before softening is introduced in the system.

Fig. 10 shows the progress of the accumulative damage versus the dynamic cycles. A comparison is presented between the damage values obtained from Miner's rule and the finite element coupled analysis. Miner's rule underestimates the damage, hence overestimates the fatigue life. It is important to mention that the 30th dynamic cycle, where there is a sharp change in the curve, corresponds to the maximum temperature of 100°C. Beyond the 30th cycle, damage does not change much as the temperature starts to cool down.

6.2. Load case II

The dynamic loading in this case is applied in the Y direction only. Fig. 11 depicts the average axial stress–axial strain (σ_y–ε_y) response in the solder joint for 5 g-10 Hz vibrations for 120 cycles. In this case, unlike case I, there is plasticity under dynamic loading alone. Subsequently it results in a low cycle fatigue. The non-

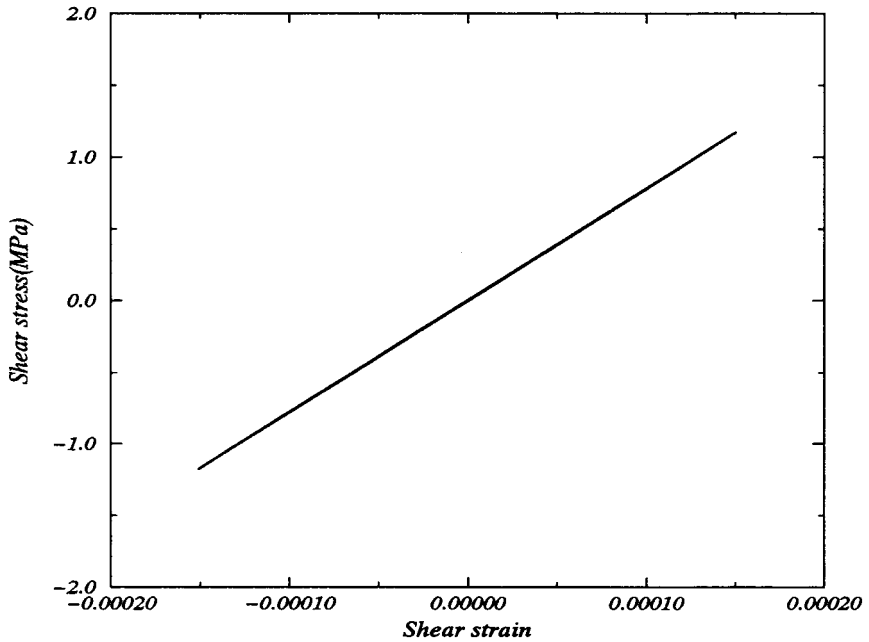

Fig. 8. Stress versus strain response for dynamic loading of 5 g-10 Hz in the X-direction.

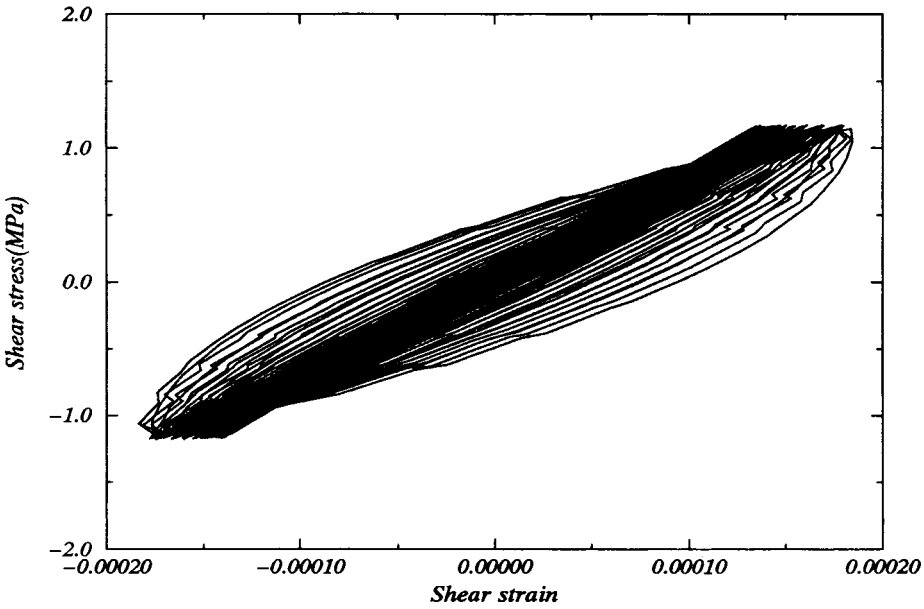

Fig. 9. Stress versus strain response for the concurrent thermal and dynamic loading (in the X-direction only).

smoothness of the response is primarily due to the boundary conditions where the package is fixed in the Y-direction only at the ends and thus is capable of significant displacements. Fig. 12 shows the (σ_y–ε_y) response of the solder joint under combined thermal and dynamic loading. Shear stress level in the solder joint during vibrations was found to be insignificant. As the temperature increases, the plastic strain starts to increase and reaches a maximum value at the highest temperature (100°C). At this temperature the hysteresis

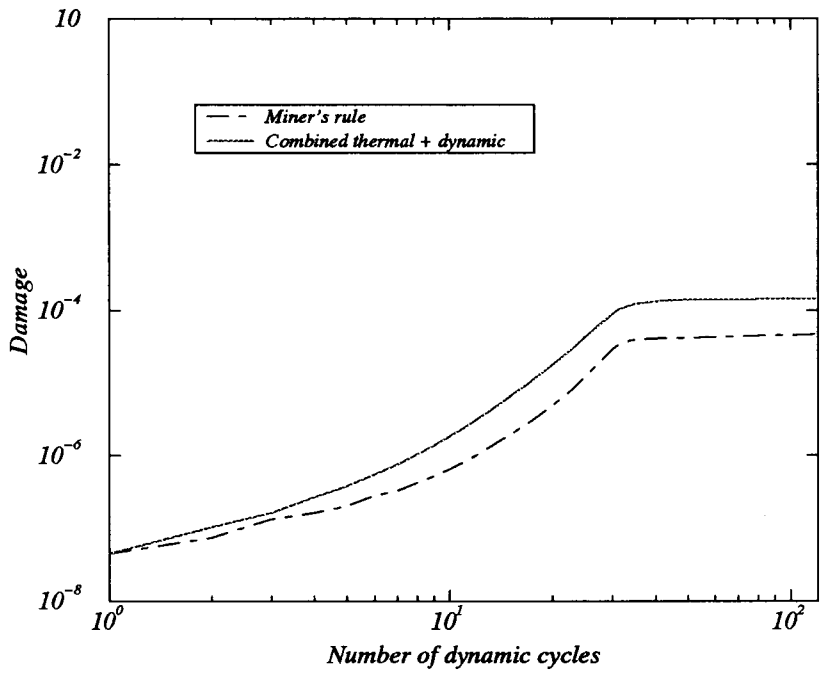

Fig. 10. Damage versus number of dynamic cycles for concurrent thermal and dynamic loading (in the X-direction only).

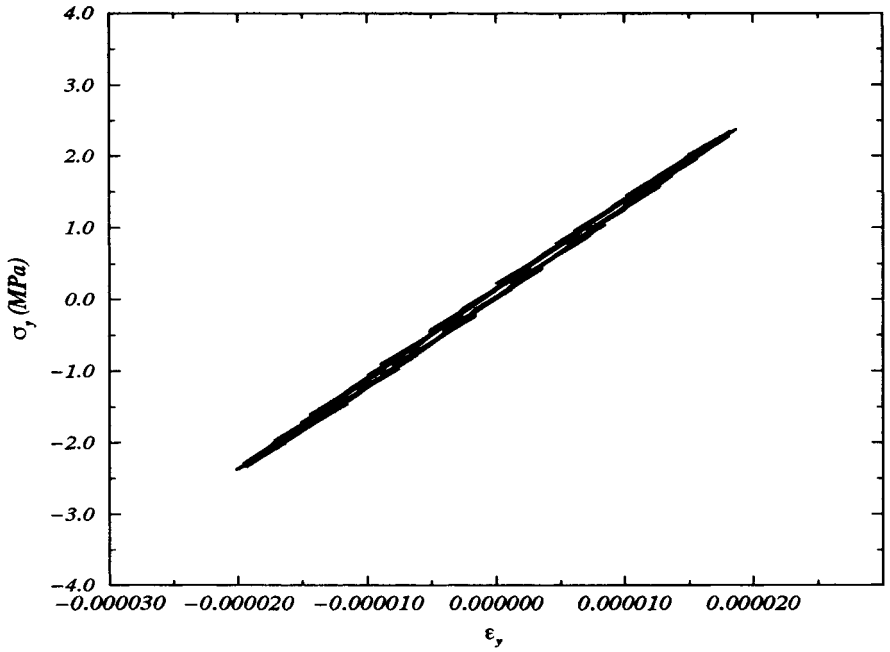

Fig. 11. Stress versus strain response for dynamic load of 5 *g*-10 Hz (in the *Y*-direction only).

curve has the largest area. As the temperature goes down again, the plastic strain is reduced and goes to a minimum value at the lowest temperature. The maximum strain level is twice as large when compared to load case I. Fig. 13 shows the damage (due to concurrent loads) versus the number of dynamic cycles. As can be seen from the figure, the damage is much larger than the application of combined thermal and dynamic loading in the *X*-direction. This is mostly because of the boundary condition imposed on the structure. The

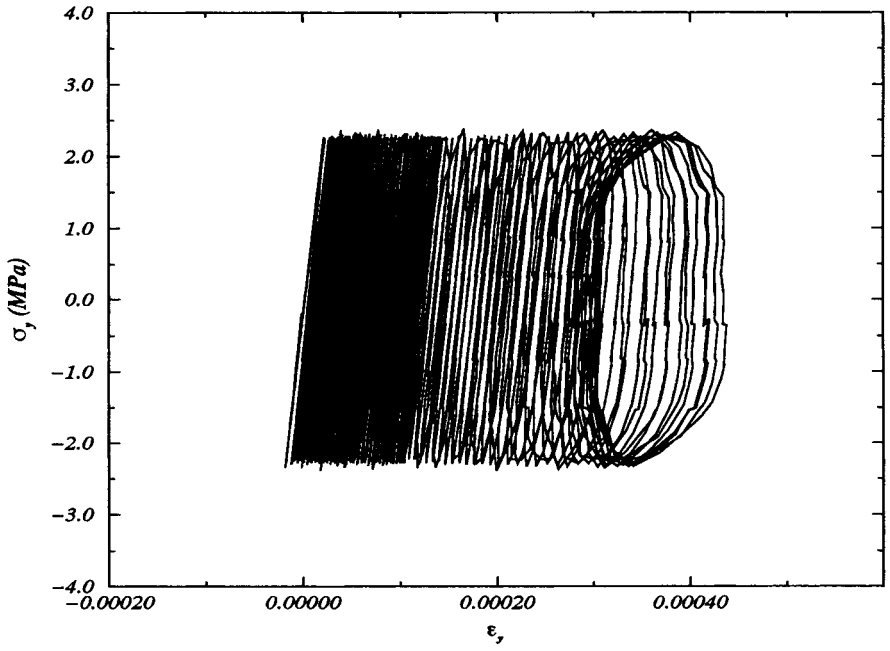

Fig. 12. Stress versus strain response for concurrent thermal and dynamic load of 5 *g*-10 Hz (in the *Y*-direction only).

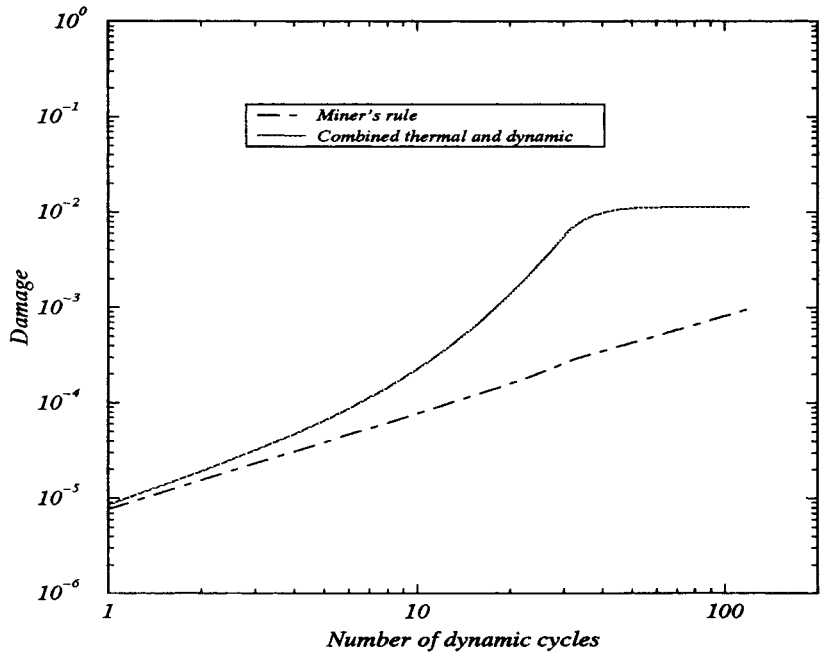

Fig. 13. Damage versus number of dynamic cycles for concurrent thermal and dynamic loading of 5 g-10 Hz (in the Y-direction only).

package is constrained only at the ends in the Y-direction and hence the central portion of the package is subjected to significant displacements, which leads to larger stress and strain in the solder joint. It is also observed that Miner's rule significantly overestimates the fatigue life.

6.3. Load case III

In this loading combination, the thermal cycling and the dynamic loading of 5 g-10 Hz are applied in both X and Y directions. Figs. 14 and 15 show τ_{xy}–γ_{xy} response and the σ_y–ε_y response, respectively, of the solder joint under dynamic loading only. Fig. 14 shows that the maximum shear stress level is almost the same as when vibrations are applied in the X-direction only. This is in spite of the fact that the energy dissipated in the joint is much larger due to the larger plastic strain. This is probably due to the contribution of the vertical displacements to the shear stress.

Fig. 16 shows the τ_{xy}–γ_{xy} response in the solder joint under concurrent thermal and dynamic loading of 5 g-10 Hz in both X and Y directions. The maximum strain level reached is also larger when compared to load cases I and II. As a result, having loading in both X and Y directions is the worst combination for this boundary condition. Another feature observed in this response is that with the reduction of temperature, the plastic strain starts to reduce but does not go to the original position at room temperature and, even at lower temperatures, stops at a certain plastic strain level.

Fig. 17 shows the σ_y–ε_y response for the concurrent thermal and dynamic loading of 5 g-10 Hz in both X and Y directions. Comparing it with cases I and II, we can conclude that combining vibrations in X and Y directions does not make any difference in the σ_y–ε_y response in the solder joint.

Fig. 18 depicts the distribution of the coupled accumulative damage versus the number of dynamic cycles for the coupled analysis and for the analysis performed using Miner's rule. An order of magnitude difference is observed when coupled analysis results are compared with Miner's rule results. Miner's rule significantly underestimates the total damage, and as a result overestimates the fatigue life. The latter observation indicates that performing a coupled analysis is essential for any final analysis. When Figs. 13 and 18 are compared, it is seen that the damage levels are close, with the damage under the concurrent thermal and dynamic loading in both X and Y directions being slightly larger than the damage under concurrent thermal and dynamic loading in the Y-direction only. So it can be concluded that for this particular boundary condition, loading in the Y-direction has a greater damaging effect on the solder joint than loading in the X-direction.

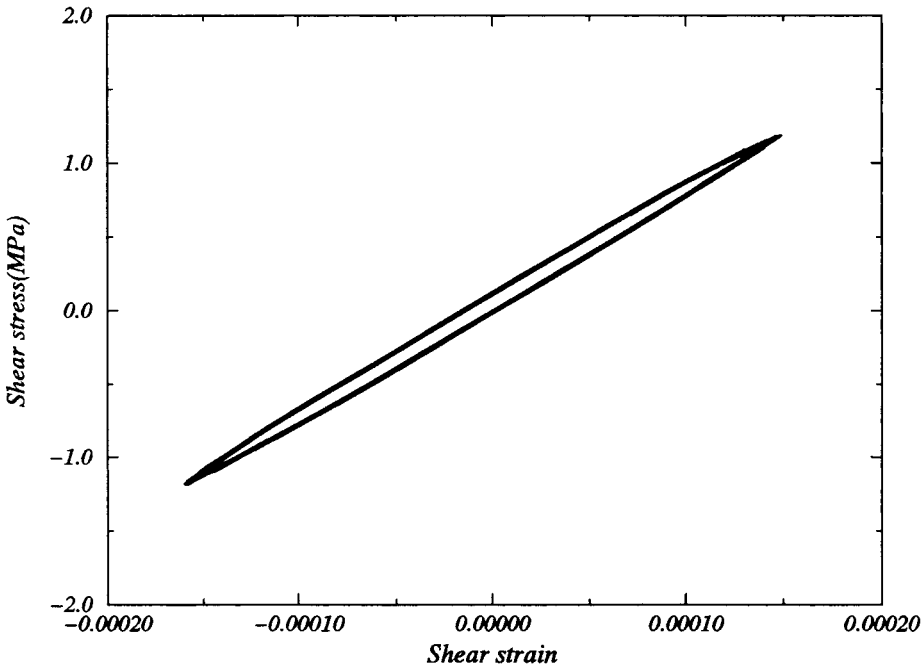

Fig. 14. Shear stress versus shear strain response for dynamic load of 5 g-10 Hz in both X and Y directions.

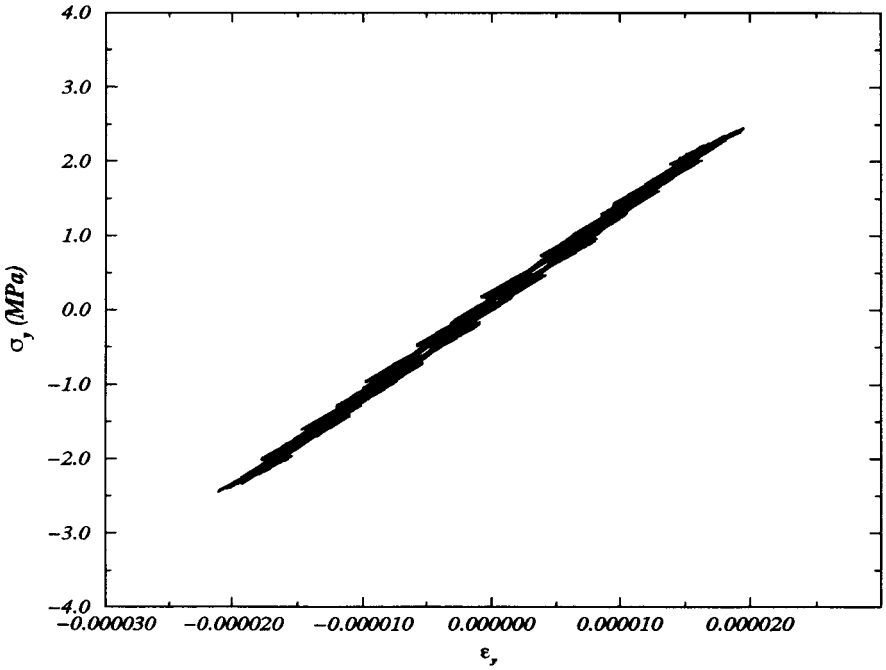

Fig. 15. Axial stress versus axial strain response for dynamic load of 5 g-10 Hz in both X and Y directions.

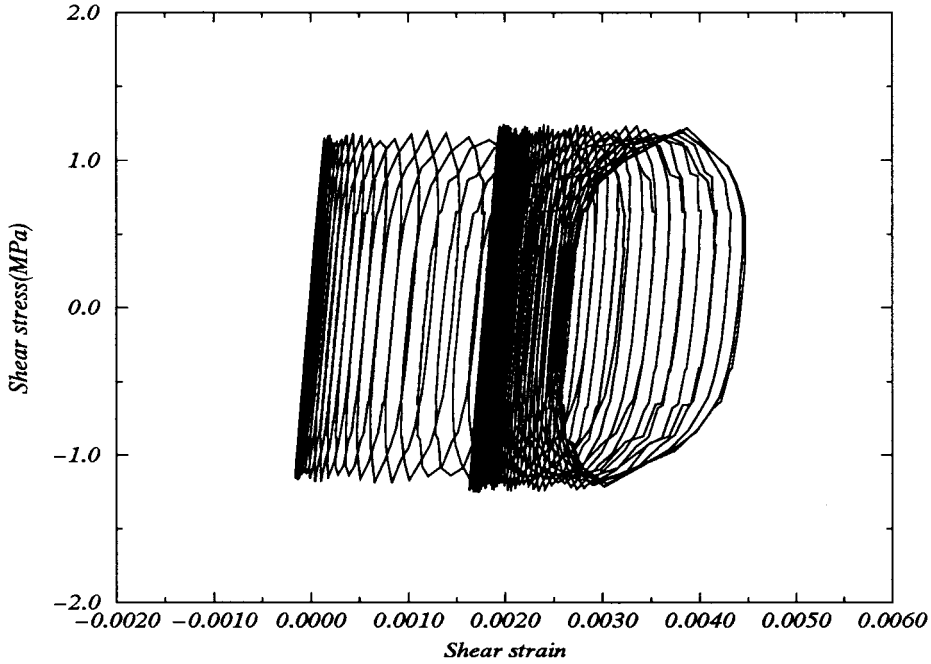

Fig. 16. Shear stress versus shear strain response for concurrent thermal and dynamic load of 5 *g*-10 Hz in both *X* and *Y* directions.

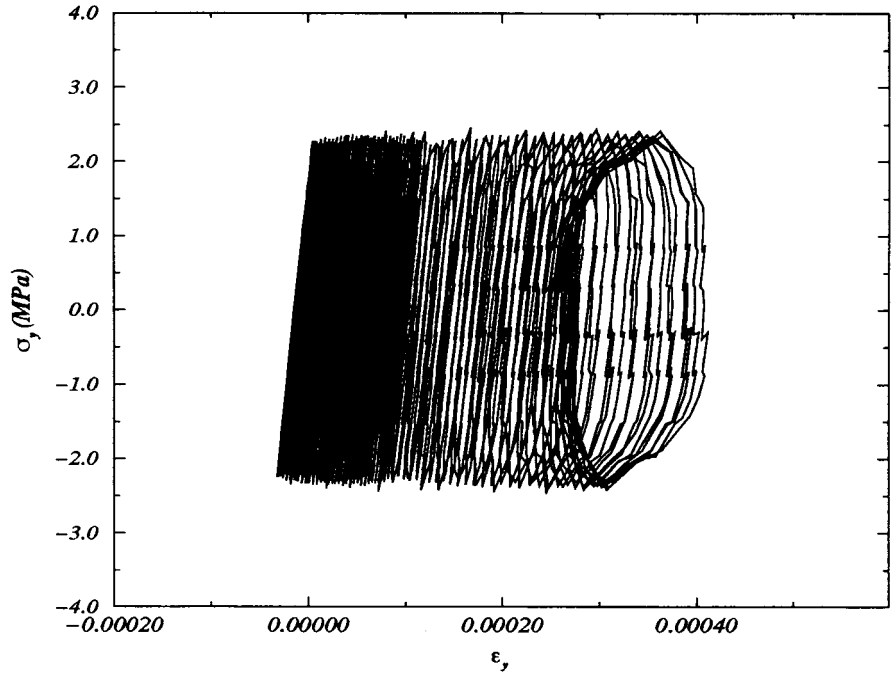

Fig. 17. Axial stress versus axial strain response for concurrent thermal and dynamic loading of 5 *g*-10 Hz in both *X* and *Y* directions.

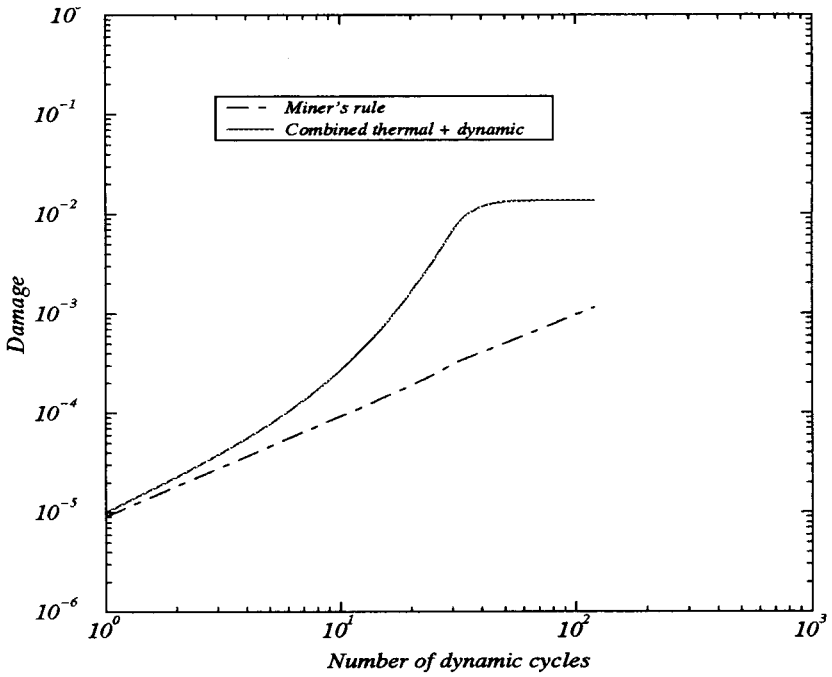

Fig. 18. Damage versus number of dynamic cycles for concurrent thermal and dynamic loading of 5 g-10 Hz in both X and Y directions.

7. Conclusion

In this paper a unified constitutive model has been proposed for fatigue life predictions of solder joints in surface mount technology electronic packaging. Coupled thermo-viscoplastic–dynamic analysis results have been compared against fatigue life predictions using Miner's rule. The comparisons indicate that Miner's rule significantly underestimates the accumulative damage in the system. The results indicate that the reliability of a solder joint cannot be solely determined by the thermal cycles experienced. It has been shown that dynamic loads can lead to low cycle fatigue without the existence of thermal loads. Obviously, the simultaneous application of thermal and dynamic loads significantly shortens the fatigue life.

In this study it has been shown that Miner's rule overestimates the fatigue life. Using Miner's rule for the preliminary analysis would be acceptable, but the final analysis should be performed for the coupled loading.

The results strongly suggest that having thermal loading in conjunction with dynamic loading makes a significant difference in the fatigue life of the solder joint.

Acknowledgements

The research results reported herein were supported by grant no. N00014-97-1-0685 from the Department of Defense Office of Naval Research Young Investigator Award Program. The Program Director for the project is Dr Roshdy Barsoum of ONR. We are grateful for his valuable comments.

References

[1] ANSYS. User's manual. Swanson Analysis Systems Inc., Version 5.3 1992.
[2] ABAQUS. User's manual. Hibbit, Karlsson and Sorrensen Inc., Version 5.6 1996.
[3] Adams PJ. Thermal fatigue of solder joints in micro-electronic devices. MS Thesis, MIT 1986.
[4] Barker D, Vodzak J, Dasgupta A, Pecht M. Combined vibrational and thermal solder joint fatigue—a generalized strain versus life approach. Trans ASME J Electron Packag 1990;112:129–34.
[5] Basaran C, Chandaroy R. Finite element simulation of the temperature cycling tests. IEEE Trans Comput Pack Manuf Technol, Part A 1997;20(4):530–6.
[6] Basaran C, Desai CS, Kundu T. Thermomechanical

finite element analysis of microelectronics packaging. Part I: theory. Trans ASME, J Electron Packag 1998;120:41–7.
[7] Basaran C, Desai CS, Kundu T. Thermomechanical finite element analysis of microelectronics packaging. Part I: verification and application. Trans ASME, J Electron Packag 1998;120:48–54.
[8] Basaran C, Chandaroy R. Nonlinear dynamic analysis of surface mount interconnects. Part I: theory, Trans ASME, J Electron Packag (in press).
[9] Basaran C, Chandaroy R. Nonlinear dynamic analysis of surface mount interconnects. Part II: applications, Trans ASME, J Electron Packag (in press).
[10] Basaran C, Yan CY. A thermodynamic framework for damage mechanics of Pb/Sn solder joints, Trans ASME, J Electron Packag (in press).
[11] Basaran C, Zaman , Booker , Gioada. Unified disturbed state concept in modeling and applications in geomechanics, Wiley, New York, (in press).
[12] Bathe KJB. Finite element procedures in engineering analysis. Englewood Cliffs, NJ: Prentice Hall, 1996.
[13] Boltzmann L. Lectures on gas theory. University of California Press, 1898 Trans. by Brush S, 1964.
[14] Chandaroy R. Damage mechanics of microelectronic packaging under combined dynamic and thermal loading. Ph.D. Dissertation, SUNY at Buffalo 1998.
[15] Clech J-P, Augis JA. Engineering analysis of thermal cycling accelerated test for surface-mount attachment reliability evaluation. In: Proceedings of the VII Annual Electronic Packaging Conference, Boston, MA, November, 1987. Vol 1. p. 385–411.
[17] Coffin Jr LF. Trans ASME 1954;Vol 76:931–50.
[18] Coffin Jr LF. Fracture 1969. London: Chapman & Hall, 1969.
[19] Cosserat E, Cosserat F. Theorie des Corps Deformables. Paris: Herman, 1909.
[20] Darveaux R, Edward Y, Turlik I, Murthy KI. Mechanical characteristics of In and Pb55Sn solders in a thinfilm multichip package. In: Materials Research Symposium Proceedings, 1991. Vol 203. p. 443–449.
[21] Dasgupta A, Oyan C, Barker D, Pecht M. Solder creep-fatigue analysis by an energy-partitioning approach. Trans, ASME J Electron Packag 1992;114:21–7.
[22] Desai C. Constitutive modeling using the disturbed state concept. In: Muhlhaus HB, editor. Continuum models for materials with microstructure. Chichester: Wiley, 1995 Chapter 8.
[23] Desai CS, Toth J. Disturbed state constitutive modeling based on stress–strain and nondestructive behavior. Int J Solids Struct 1996;33:1619–50.
[24] Desai CS, Chia J, Kundu T, Prince JL. Thermomechanical response of materials and interfaces in electronic packaging: Part I—unified constitutive model and calibration. J Electron Packag 1997;119:294–306.
[25] Frear D, Morgan H, Burchett S, Lau J. The mechanics of solder alloy interconnects. New York: Chapman & Hall, 1994.
[26] Frear DR, Burchet SN, Rashid MM. A microstructurally based model of solder joints under conditions of thermo-mechanical fatigue. Adv Electron Packag ASME 1995;EEP(10):347–60.
[27] Guo Q, Cutiongco EC, Keer LM, Fine ME. Thermomechanical fatigue life prediction of 63Sn/37Pb solder. Trans ASME, J Electron Packag 1992;114:145–51.
[28] Halliday D, Resnick R. Physics. New York: Wiley, 1966.
[29] Huang JH, Pei JY, Qian YY, Jiang YH. Life predictions of SMT solder joints under thermal cycling. Soldering Surface Mount Technol 1994;16:31–50.
[30] Hill R. The mathematical theory of plasticity. Oxford: Oxford University Press, 1950.
[31] Ishikawa H, Sasaki K. Constitutive model for 60Sn-40Pb solder under cycling loading. In: Chen WT, Abe H, editors. Advances in electronic packaging, Proceedings of Joint ASME/JSME Conference on Electronic Packaging, 1992. Vol 1. p. 401–408.
[32] Ju SH, Kuskowski S, Sandor BI, Plesha ME. Creep-fatigue damage analysis of solder joints. In: Schroeder SA, Mitchell MR, editors. Fatigue of electronic materials, STP–1153. Philadelphia, PA: American Society for Testing and Materials, 1994. p. 1–21.
[33] Kashyap BP, Murty GS. Experimental constitutive relations for the high temperature deformation of a Pb-Sn eutectic. Mater Sci Engng 1981;50:205–13.
[34] Knecht S, Fox LR. Constitutive relation and creep-fatigue life model for eutectic tin–lead solder. IEEE Trans Comp Hybr Manuf Technol 1990;13:424–33.
[35] Lau J, Erasmus S. Reliability of fine pitch plastic quad flat pack leads and solder joints under bending twisting and thermal conditions. Trans ASME, J Elec Packag 1993;115:322–8.
[36] Manson SS. Behavior of materials under conditions of thermal stress. In: Heat Transfer Symposium, University of Michigan, 27–28 June, 1952. University of Michigan Press, 1953.
[37] Manson SS. Mech Des 1960;32(14):139–44.
[38] Miner MA. 1945 Cumulative damage in fatigue, ASME J. Appl Mech.
[39] Oshida Y, Chen P. High and low-cycle fatigue damage evaluation of multilayer thin film structure. Trans ASME, J Electron Packag 1991;113:14–20.
[40] Owen DRJ, Hinton E. Finite elements in plasticity. Swansea: Pineridge Press, 1980.
[41] Pan T. Thermal cycling induced plastic deformation in solder joints: Part III: strain-energy based fatigue life model and effects of ramp rate and hold time. In: Proceedings of the ASME Winter Annual Meeting, 1–6 December, Atlanta, GA, 1991.
[42] Pao YH, Govila R, Badgley S, Jih E. An experimental and finite element study of thermal fatigue fracture of PbSn solder joints. Trans ASME J Electron Packag 1993;115:1–8.
[43] Ross RG, Wen LC, Mon GR, Jetter E. Solder creep-fatigue interactions with flexible leaded parts. Trans ASME, J Electron Packag 1992;114:185–92.
[44] Sauber J, Seyyedi. Predicting thermal fatigue lifetimes for SMT solder joints. Trans ASME, J Electron Packag 1992;114:472–6.
[45] Schmidt CG. A simple model for fatigue of leadless cer-

amic chip carrier solder attachments. J Electron Manuf 1992;2:31–6.

[46] Skipor A, Harren S, Botsis J. Constitutive characterization of 63/37 Sn/Pn eutectic solder using the Bodner–Partom unified creep-plasticity model. In: Chen W.T., Abe H., editors. Advances in Electronic Packaging, Proceedings of the Joint ASME/JSME Conference on Electronic Packaging, 1992. Vol 2. p. 661–672.

[47] Solomon HD, Tolksdorf ED. Energy approach to the fatigue of 60/40 solder: Part II—influence of hold time and asymmetric loading. Trans ASME, J Electron Packag 1996;118:67–71.

[48] Subrahmanyan R, Wilcox JR, Li C. A damage integral approach to thermal fatigue of solder joints. IEEE Trans Components, Hybrids, Manuf Technol 1989;12.

[49] Suhir E, Lee YC. Thermal, mechanical and environmental durability design methodologies. In: Electronics materials handbook, , vol. Vol 1. ASM International, 1988.

[50] Steinberg DS. Vibration analysis for electronic equipment. New York: Wiley, 1988.

[51] Tien JK, Headrix BC, Attarwala AI. Understanding the cyclic mechanical behavior of lead/tin solder. Trans ASME, J Electron Packag 1991;113:42–8.

[52] Verma S, Dasgupta A, Barker D. A numerical study of fatigue life of J-leaded solder joints using the energy partitioning approach. Trans ASME, J Electron Packag 1993;115:416–23.

[53] Zubelewicz A, Guo Q, Cutiongco EC, Fine ME, Kheer LM. Micromechanical method to predict fatigue life of solder. Trans ASME, J Electron Packag 1990;112:7–14.